INVESTIGATION OF SQUEEZE-FILM DAMPERS IN FLEXIBLE SUPPORT STRUCTURES

R. Holmes and M. Dogan
University of Sussex
Brighton, England BNL 9QT

SUMMARY

Squeeze-film dampers are a means of curing instabilities in rotating-shaft assemblies. Their efficiency depends very much on the condition of the oil, which in turn depends on inlet and outlet arrangements, on damper geometry and on the flexibility of the rotor and surrounding structure. The work discussed in this paper concerns rig investigations in which structural flexibility is included experimentally and comparisons are made between measured and predicted results.

INTRODUCTION

In two previous papers (refs. 1 and 2), the performance of a squeeze-film damper unassisted by any retainer spring was examined when interposed between a rigid rotor and its rigid bearing pedestals. In many gas turbine applications, however, both rotor and pedestals are flexible, the latter to the extent that the first two rotor-pedestal critical speeds are essentially bounce modes, in which the rotor does not bend to any significant degree. Instead, on increase in speed the rotor often vibrates first in a symmetric and then in an anti-symmetric mode, while the pedestals are the only elements to show any appreciable degree of dynamic deflection. For such systems a squeeze-film damper interposed between one or more of the rolling-element bearings of the rotor and the pedestals can contribute a degree of damping which may enable the passage of the system through such critical speeds without vibration becoming excessive, and inhibit possible rotational instability.

It is not uncommon in gas turbines for the antisymmetric mode of vibration to exhibit a node near one of the rolling-element bearings. With such an application in mind, a test rig (fig.1) was designed and built, which afforded the investigation of the squeeze-film damper 1 at one of its two rolling-element bearings 2, the other bearing 3 being of the self-aligning variety. This constituted a pivot about which an antisymmetric (i.e. conical) mode of vibration would occur, when the rotor 4 was acted upon by a force arising from rotation of the unbalance mass 5 . The test rig was provided with flexible bars 6, which simulated the pedestal flexibility of an actual engine. Alternatively, the housing 7 could be clamped by the special clamps 8 to afford investigation of the squeeze-film damper alone. A heavy foundation block 9 was provided which represented ground and into which the flexible bars were screwed. Oil of 21 cp viscosity was supplied to the damper via three supply holes 10 and a central circumferential groove (fig.2). End plates were attached at the

* Performed under contract to Rolls Royce Limited, England

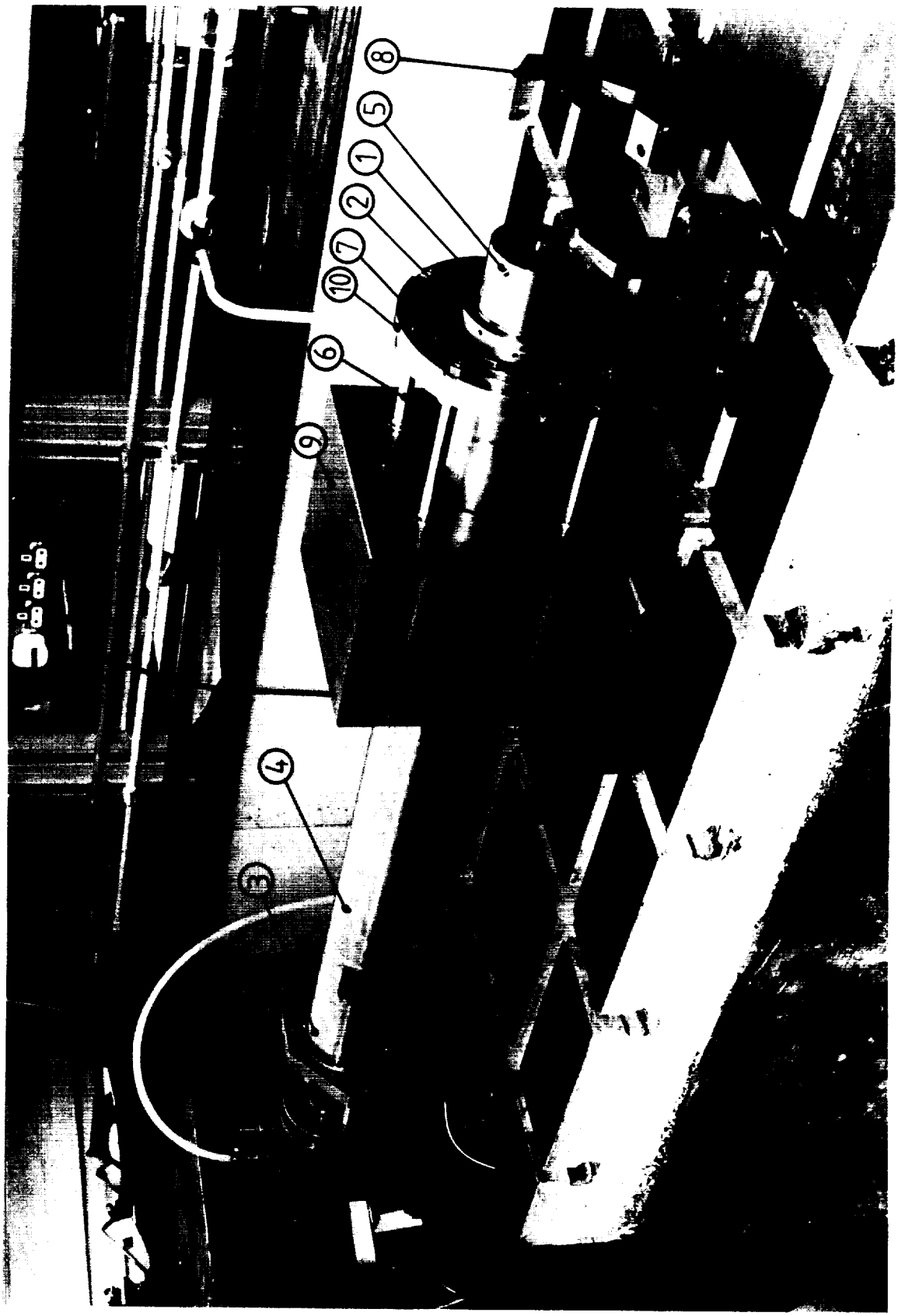

Figure 1. - Damper test rig.

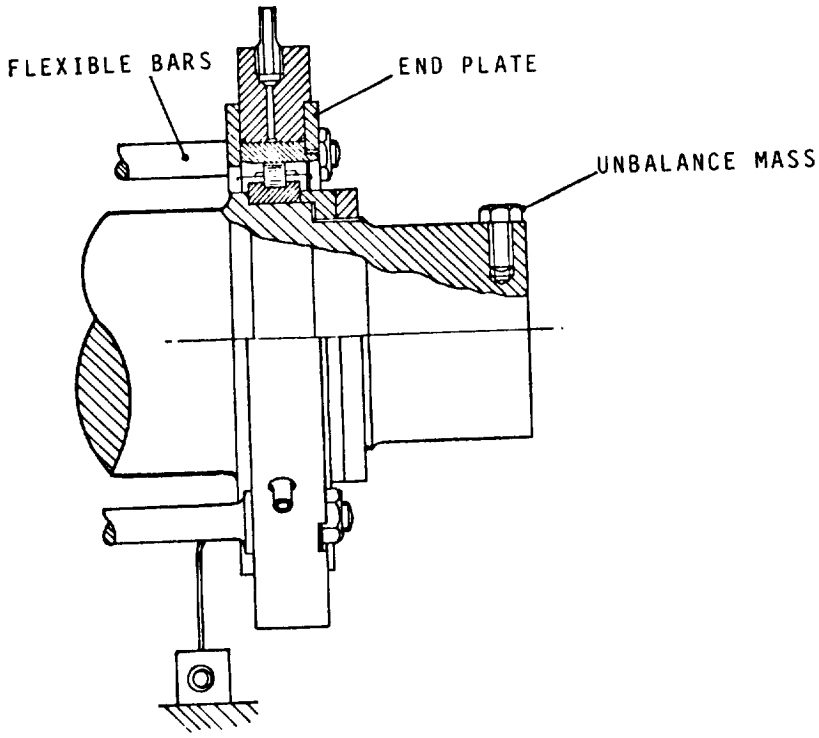

Figure 2. - Detail of damper.

ends of the outer element of the damper to afford some sealing, the extent of which could be varied by the insertion of spacing shims. The squeeze-film dimensions were set by the outer diameter of the rolling bearing (136 mm), the damper land length (9 mm) and its radial clearance (.216 mm).

Proximity vibration pickups were used to measure the vibration of the shaft relative to the pedestal and relative to ground. A pressure transducer was placed at a mid-land position at the base of the squeeze film to measure dynamic pressure in the oil under operating conditions and a thermocouple was also provided there to record oil-film temperature. The presence of the flexible bars allowed convenient recording of transmitted force by the provision of strain gauges.

This paper describes investigations into the performance of the dampers and a comparison of experimental findings with numerical predictions. For the latter, the numerical method developed in reference (2) was used. This was based on the short-bearing approximation applied to the Reynolds equation to describe the pressure field in the squeeze film and required the clearance between the end plates and the inner member of the damper to be wide enough to enable the assumption of atmospheric pressure at the ends of the damper to be used.

In reference (2) it was shown that the independent parameters of the squeeze-film damper could be presented in terms of three non-dimensional groups, namely

$$Q = P/mc\omega^2$$

$$Q_c = P_c/mc\omega^2$$

and

$$\beta = \frac{\eta R}{m\omega} \cdot \left(\frac{\ell}{c}\right)^3 ,$$

in which P is the static load, usually provided by gravity, which for one land of the damper was 147 N, m is the effective mass of the rotor at each land (12.25 kg), c is the radial clearance in the damper (0.216 mm), R is the radius of the inner member of the damper (68 mm), ℓ the damper land length (9 mm) and η the oil viscosity (21 cp). ω is the rotational speed of the shaft carrying the unbalance mass, which provides the required dynamic force, P_c, causing vibration. An essential requirement in the numerical computations is the specification of a cavitation pressure below which the pressure field is curtailed. This pressure was found experimentally.

TESTS WITH CLAMPED HOUSING

Firstly a series of tests was carried out with the housing clamped and details of these are given in Table 1.

TABLE 1. - TESTS WITH HOUSING CLAMPED

Q_c	Rotor speed rev/min		
0.229	4000	4500	5000
0.642	3000	3400	3750

As the value of Q_c was increased the top speed of the rig was successively reduced in order to avoid excessive vibration of the rolling-element bearing in the damper clearance space. The value of speed dictated the corresponding values of the non-dimensional groups Q and β and these are given with the appropriate experimental recordings and numerical predictions shown later. An oil supply pressure of 34.48 KN/m^2 (5 lbf/in^2) was used throughout these tests to avoid excessive outflow from the ends of the damper through the rather wide end-plate clearances of 1.25 mm.

A set of experimental vibration orbits and pressure recordings is given in figure 3a for Q_c = 0.229. Fig. 3b shows the corresponding numerical predictions. Each numerical hydro-dynamic pressure distribution was curtailed at its experimentally-observed negative pressure limit before integration to obtain the squeeze-film forces which acted on the rotor to produce the orbit of vibration. Figures 4a and b show similar comparisons for a higher value of Q_c of 0.642, and are typical of many others.

Some significant general observations can be made from these comparisons. In figure 3a, the general sizes and dispositions of the vibration orbits are well predicted, while both the experimental and numerical recordings show a reversal in position of the sharp 'tail' between 4500 and 5000 rev/min. The pressure waveforms also show good agreement in respect of general shape and height. The orbits of figure 4a are quite well predicted in general shape, size and disposition (even to the extent of showing a sudden increase in size between 3700 and 3750 rev/min). Whilst the experimental pressure waveform at 3000 rev/min is fairly well predicted, the waveform at 3400 rev/min does not show such good agreement in that numerical computations indicate a sharp positive pressure spike, which is not reproduced experimentally. It seems probable that the slightly shallower slopes of the experimental vibration orbits do not give rise to such pressures, which are very sensitive to orbit shape. An inspection of the second experimental pressure peak in a given cycle will, however, indicate a good comparison with the numerical prediction.

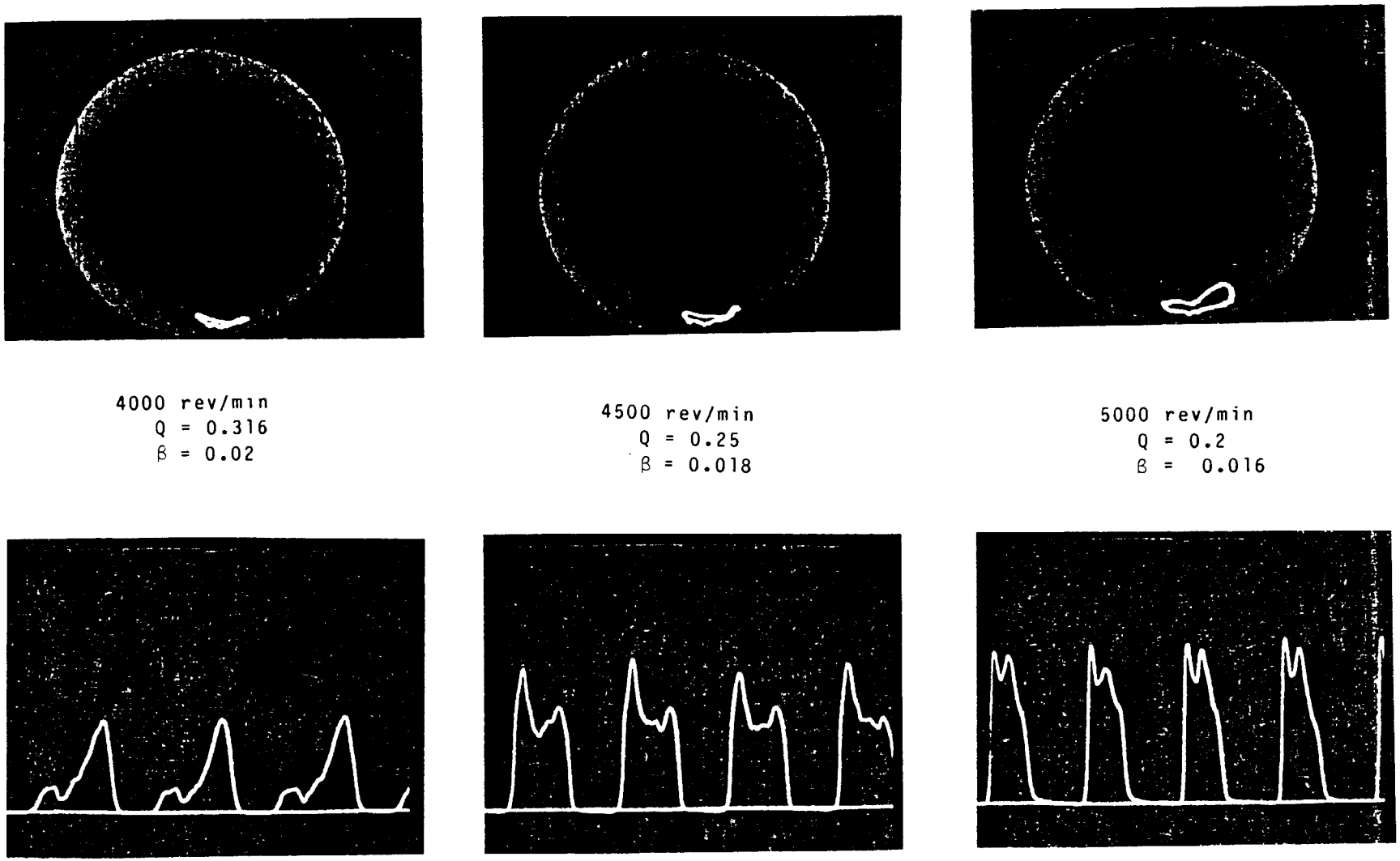

Figure 3(a). - Experimental orbits and pressure recordings (1 cm = 127 psi = 876 kN/m^2). Q_c = 0.229.

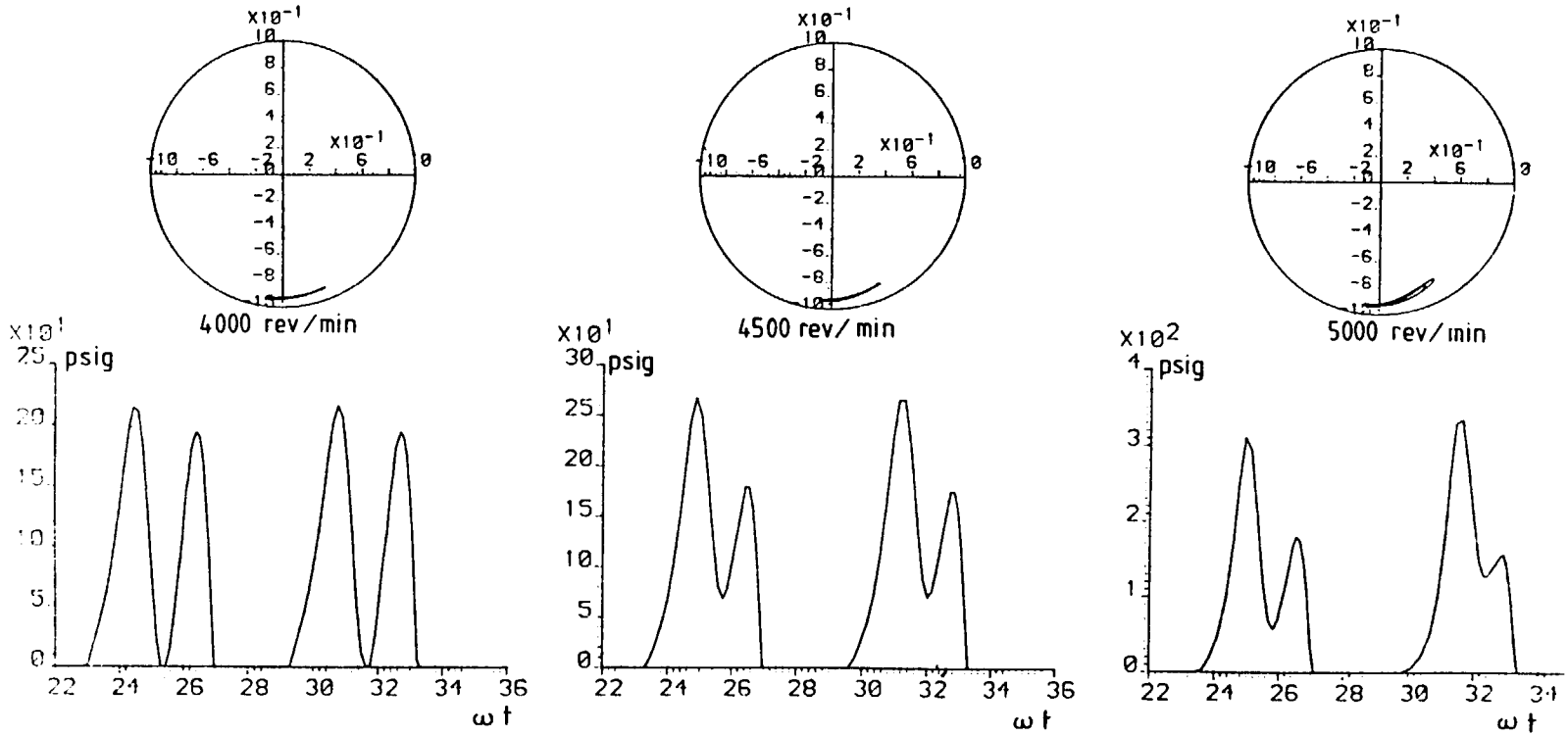

Figure 3(b). - Numerical orbits and pressures. Q_c = 0.229.

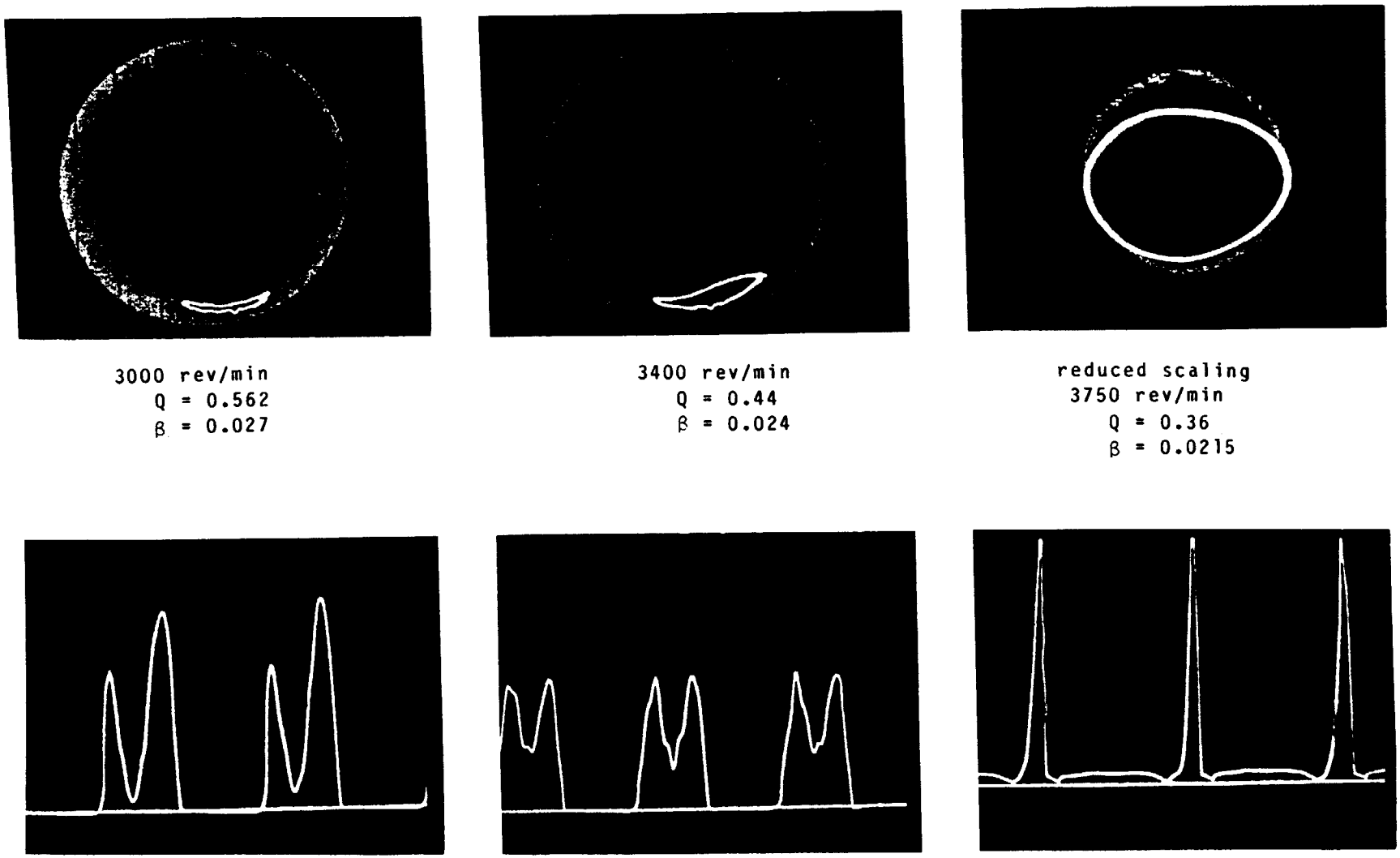

3000 rev/min
Q = 0.562
β = 0.027

3400 rev/min
Q = 0.44
β = 0.024

reduced scaling
3750 rev/min
Q = 0.36
β = 0.0215

Figure 4(a). - Experimental orbits and pressure recordings (1 cm = 127 psi = 876 kN/m^2). Q_c = 0.642.

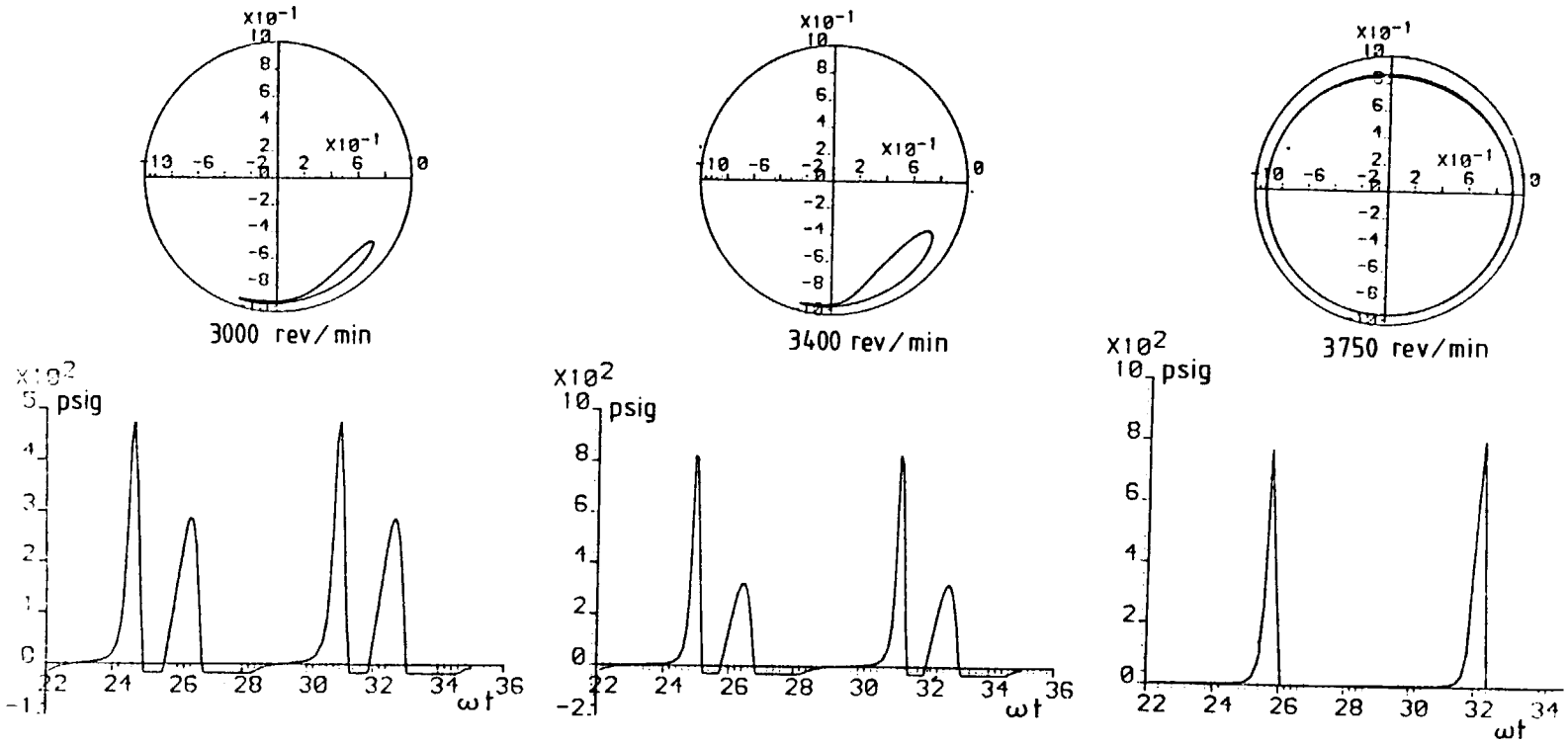

Figure 4(b). - Numerical orbits and pressures. Q_c = 0.642.

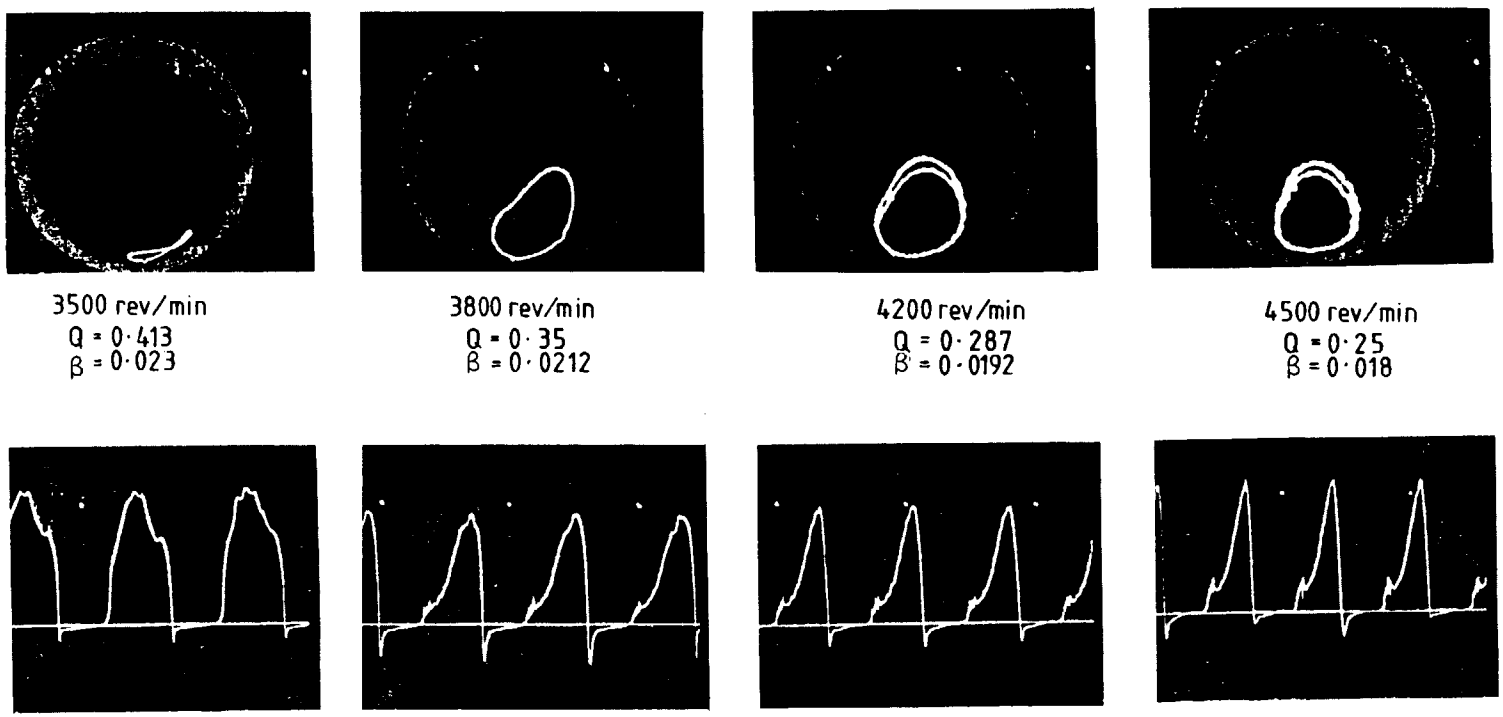

Figure 5(a). - Experimental orbits and pressure recordings (1 cm = 181 psi 1251 kN/m^2). Q_c = 0.229.

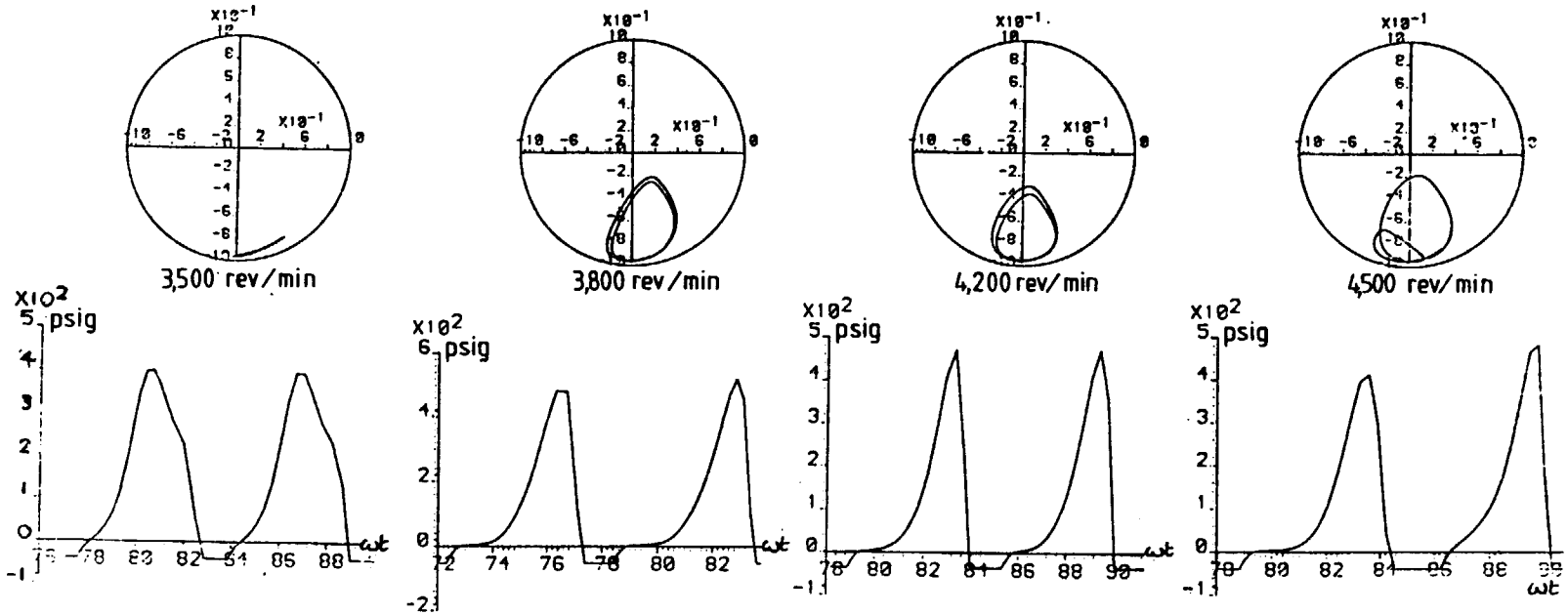

Figure 5(b). - Numerical orbits and pressures. Q_c = 0.229.

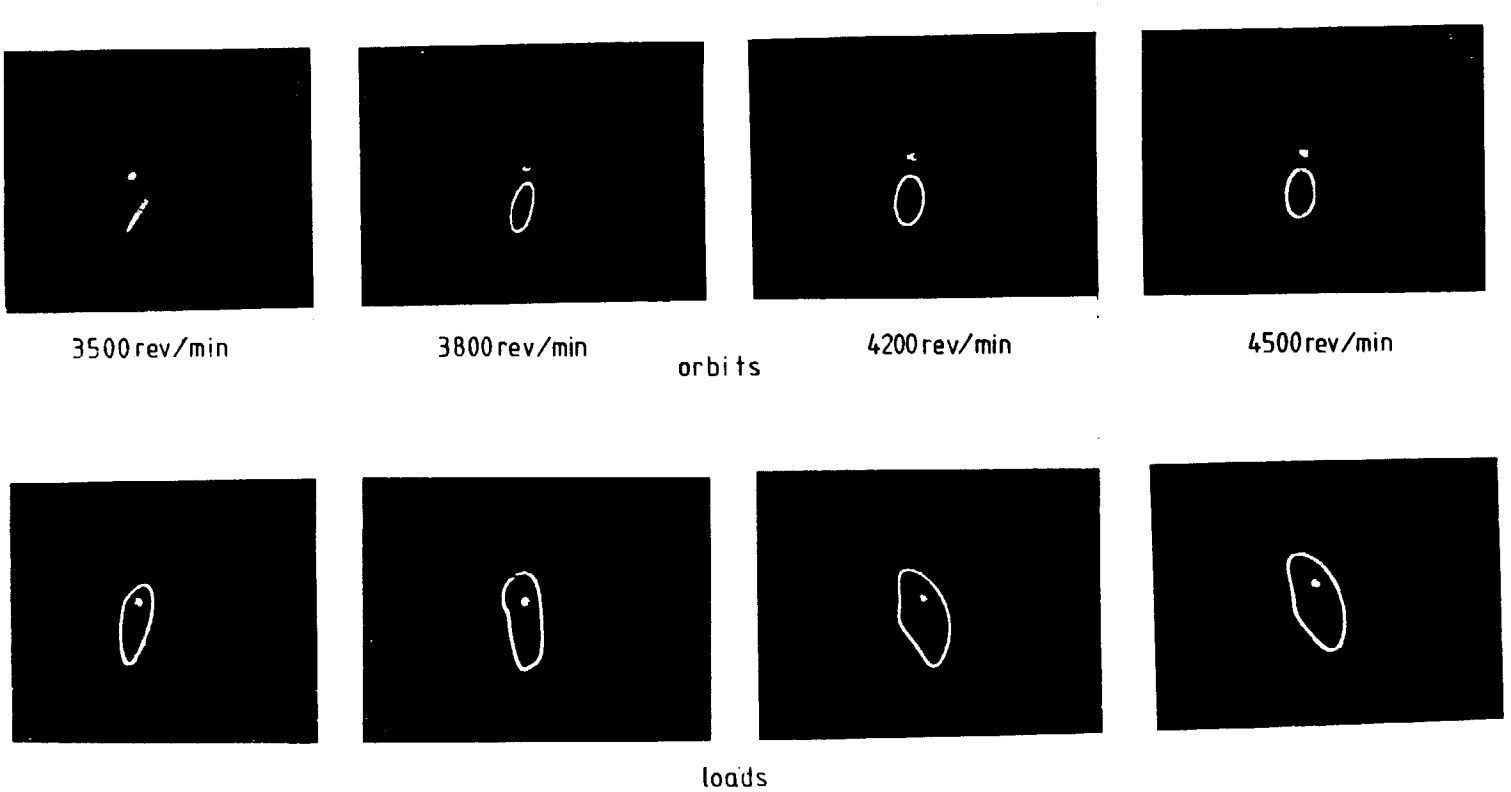

Figure 6(a). - Experimental orbits relative to ground and polar load diagrams. Q_c = 0.229. (1 cm = 0.5 mm and 1 cm = 1070 N).

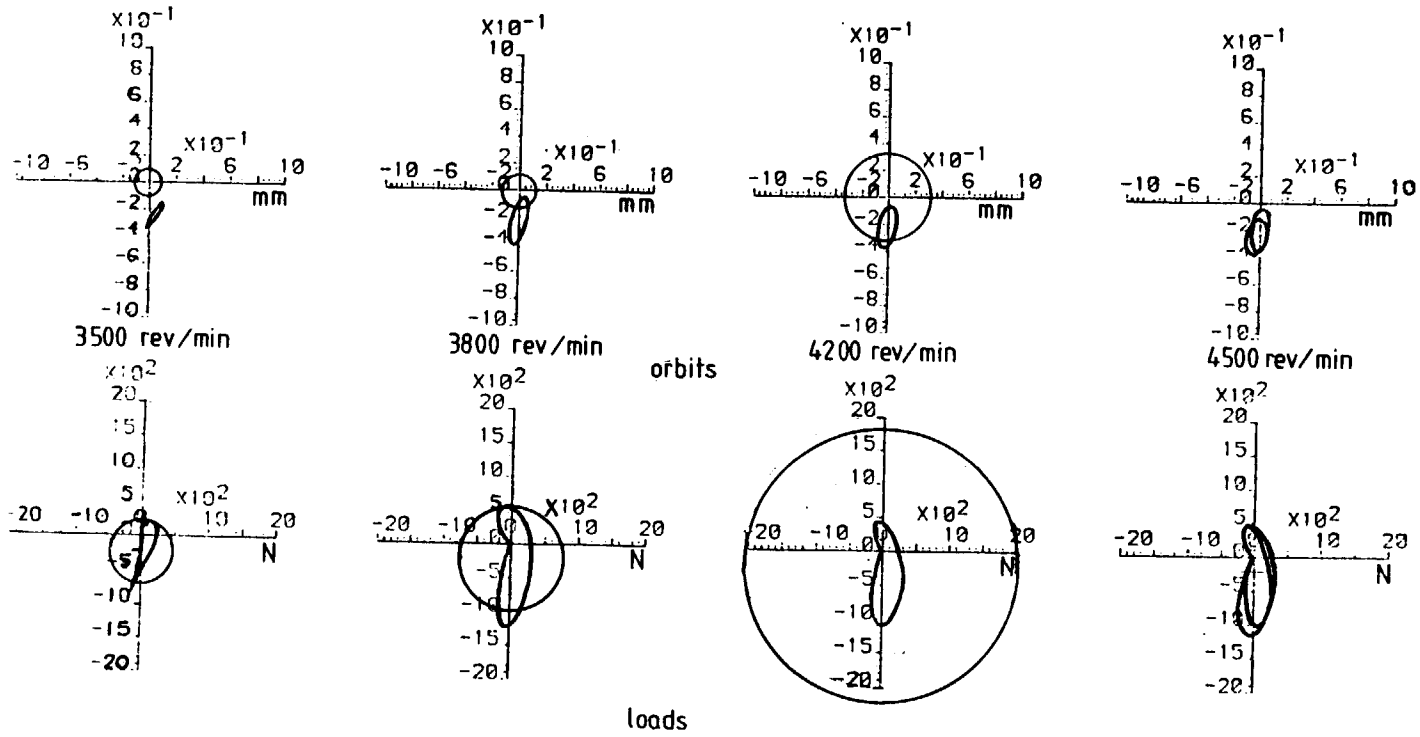

Figure 6(b). - Numerical orbits and loads. Q_c = 0.229.

TESTS WITH FLEXIBLY MOUNTED HOUSING

The housing was now unclamped, giving an undamped natural frequency of the system of about 4500 c/m. A series of tests was carried out using a Q_c value of 0.229 at speeds of 3500, 3800, 4200 and 4500 rev/min. In addition to obtaining vibration orbits of the rotor relative to the housing,orbits of the rotor relative to ground and polar diagrams of transmitted force were obtained. For such a configuration the mathematical model for the structure included the same damper model as previously, together with the stiffness of the bearing pedestal, but for speed of computation, neglected the relatively small housing mass which was only 14% of the effective rotor mass.

Comparisons of experimental and numerically predicted orbits are shown in figures 5 a,b and indicate good agreement. For the case of 3500 rev/min, a distorted figure of eight pattern is observed in both experimental and numerical recordings. The double loops visible in the other experimental recordings persisted over the entire periods of experimentation and those in the numerical predictions persisted up to a non-dimensional time ωt of 96, that is about 15 revolutions, when the length of computing time became prohibitive. The general sizes, shapes and dispositions show good agreement, and the size at 4200 rev/min is observed to be larger than at the undamped natural frequency of 4500 rev/min. The pressure recordings of figure 5b also show fair agreement in shape and size. Negative 'spikes' are evident in figure 5a, indicating that the oil can temporarily support tensile forces. Such tensile forces have been discussed in reference 2.

Turning now to the vibration orbits of the rotor relative to ground (figs. 6a,b), very good agreement prevails both in size, shape and disposition and a peak vibration between 4200 and 4500 rev/min is again observed. This suggests that the squeeze-film damper has had some effect in reducing the critical speed of the system. The polar diagrams of total dynamic load transmitted from both lands show striking agreement in many respects, such as size, shape and disposition. In particular the kink in each experimental polar diagram for 3800, 4200 and 4500 rev/min is predicted by numerical computation. These latter results give extra confidence in accepting the short bearing model of reference 2 for the squeeze film, albeit with a negative pressure curtailed at an experimentally recorded limit.

Also shown in figure 6b are circles representing total displacements and transmitted forces when no damper is present. The effect of gravity on the flexible bars increased displacements by about 0.04 mm and all forces by about 274 N. It can be seen that, at the lower speeds the damper is not really beneficial. However, at speeds approaching the critical speed, its benefits become apparent, especially at the undamped critical speed of 4500 rev/min where, without the damper the amplitudes of vibration and transmitted force would theoretically be infinite.

CONCLUSIONS

Continuing on from experience gained on test rigs involving open-ended squeeze-film dampers interposed between rigid rotors and rigid bearing pedestals (refs.1,2), this paper has described experimental and numerical work on weakly sealed dampers with flexible pedestals. Good agreement has been observed between experimental observations and numerical predictions over a wide range of operating parameters. These observations included vibration of rotor relative to bearing housing and relative to ground, dynamic pressure in the squeeze-film damper and transmitted force to ground. The work shows that, given the correct interpretation of boundary conditions in the

damper, reliance can be placed on a mathematical model incorporating the short-bearing approximation. The benefits of such a damper can also be readily seen.

This work will shortly be extended to include the effect on the damper of tighter sealing and the use of higher supply pressures and very low oil viscosities, in keeping with present-day operational practice with gas turbines.

REFERENCES

1. Humes,B. and Holmes,R.: The role of sub-atmospheric film pressure in the vibration performance of squeeze-film bearings. Jnl Mech.Eng.Sci., vol.20, no.5, pp.283-289.

2. Holmes,R. and Dede,M.: Dynamic pressure determination in a squeeze-film damper. Proc.I.Mech.E. Paper C260/80. Second International Conference on Vibrations in rotating machinery. Cambridge, Sept. 1980.

ADDITIONAL MATERIAL PRESENTED AT THE WORKSHOP

Linear theory as a qualitative predictor

Although the squeeze-film bearing is a highly non-linear element, it is worth examining its contribution to the damping of a system against a linear assessment.

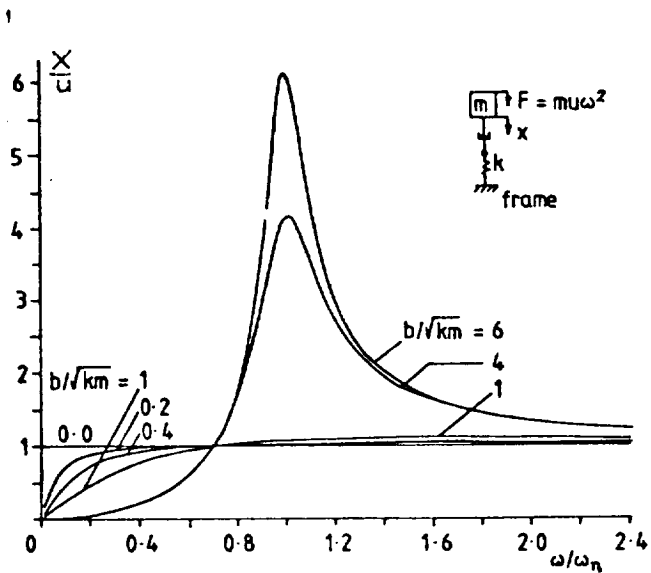

Figure 7(a). - Rotor vibration amplitude relative to the engine frame.

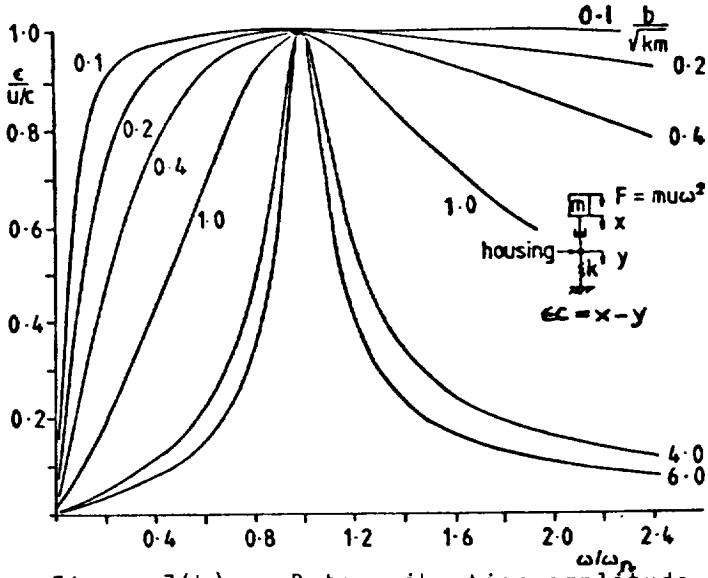

Figure 7(b). - Rotor vibration amplitude relative to the bearing housing.

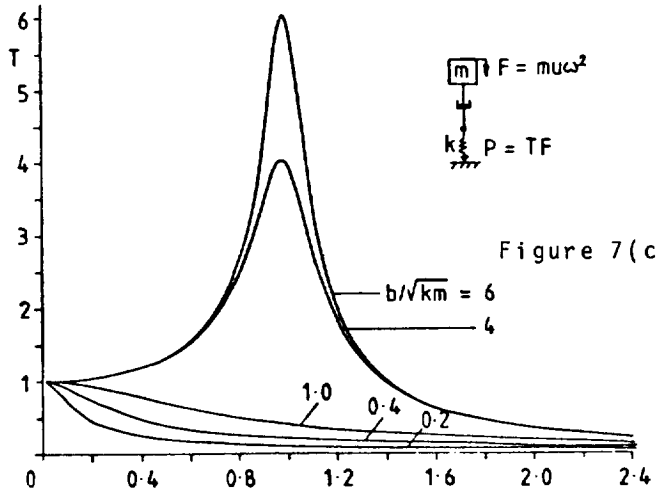

Figure 7(c). - Transmissibility.

If we consider a linear structure consisting of a series combination of mass, damper and spring, the graphs shown in Fig.7 are readily obtained. The most notable features of these graphs are, in Fig. 7a, the cross-over point $(1/\sqrt{2}, 1)$, and the increase in vibration amplitude with damping at a frequency ratio of 1; in Fig.7b, the independence of vibration with damping at $\omega/\omega_n = 1$; in Fig. 7c, the increase in transmissibility with damping at $\omega/\omega_n = 1$.

Figs. 8a, b, c show results obtained from the test rig when running at the critical speed of 4500 rev/min i.e. $\omega/\omega_n = 1$. In these figures, damping is increased in three separate ways:

i) by tightening the end sealing (Fig. 8a)
ii) by increasing the lubricant viscosity from 6 to 21 cp (Fig.8b)
and iii) by increasing the lubricant supply pressure from 5 to 45 psi (Fig.8c).

In each of these figures the photographs may be identified as follows:

a) Vibration orbit relative to bearing housing
b) Vibration orbit relative to ground
c) Pressure recording
d) Polar load diagram of transmitted force.

It may be seen that in all cases the results support the qualitative conclusion of the linear treatment, namely that at the critical speed an increase in damping by whatever means results in an increase in rotor vibration relative to ground, and an increase in transmissibility, but little change in the rotor vibration relative to the squeeze-film container.

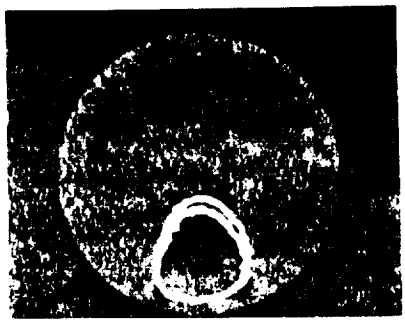

(a)

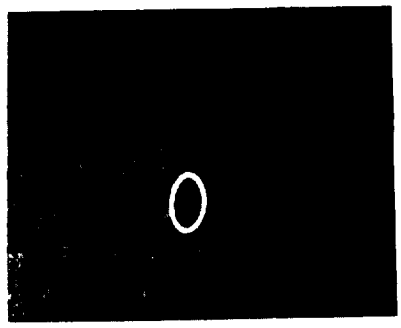

(b)

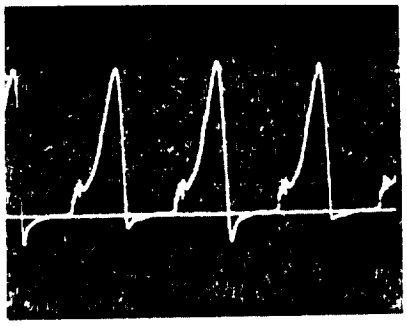

(c)

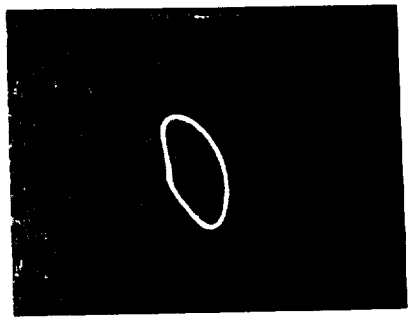

(d)

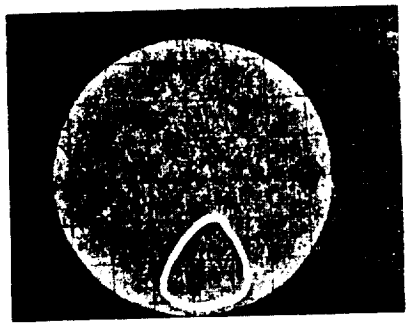

(a)

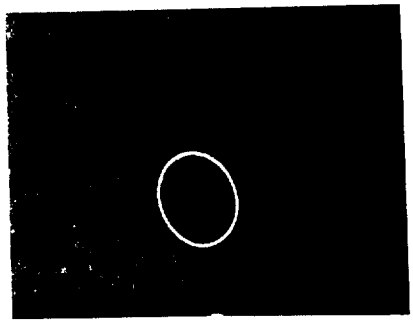

(b)

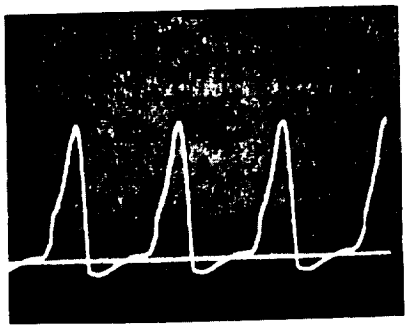

(c)

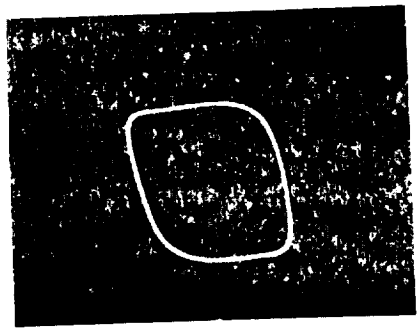

(d)

Figure 8(a). - Effect of sealing.

Upper four figures loose sealing
Lower four figures tight sealing

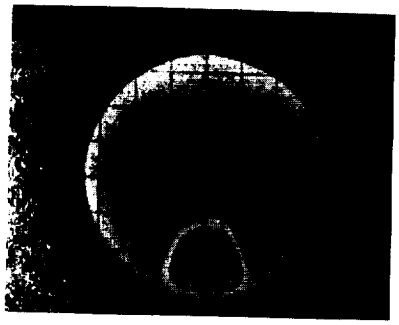

(a)

(b)

(c)

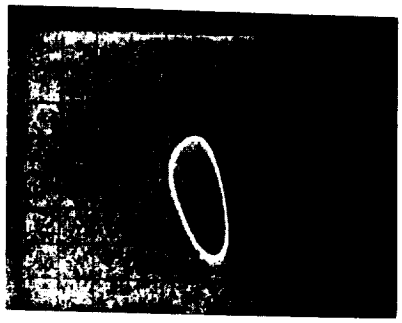

(d)

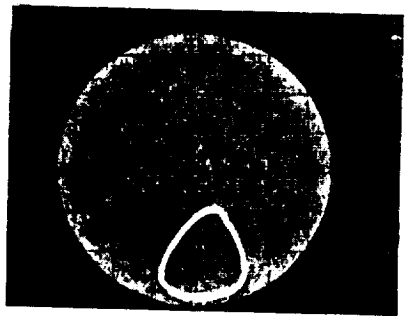

(a)

(b)

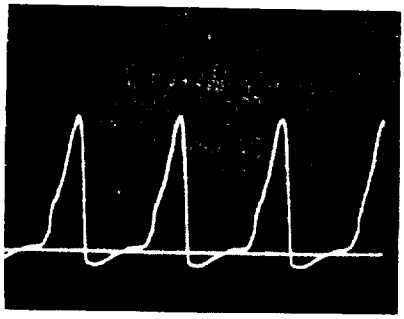

(c)

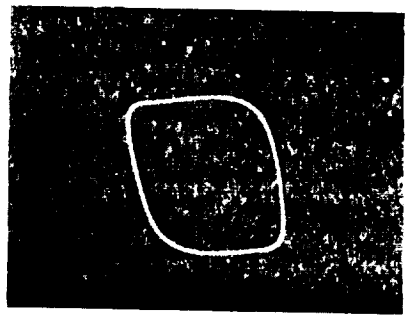

(d)

Figure 8(b). - Effect of lubricant viscosity.

Upper four figures 6 cp
Lower four figures 21 cp

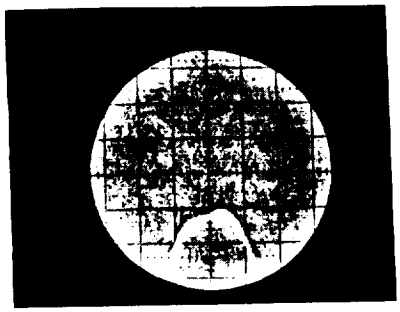

(a)

(b)

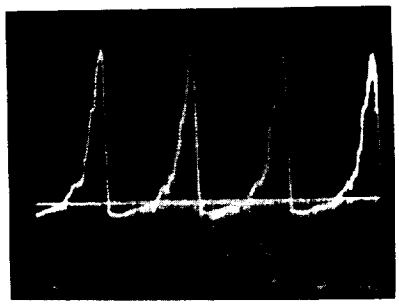

(c)

(d)

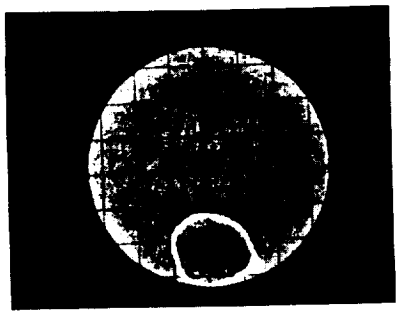

(a)

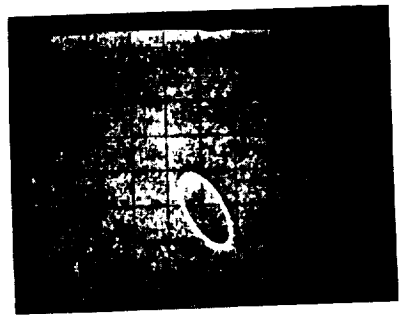

(b)

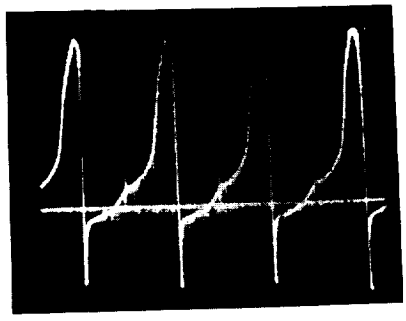

(c)

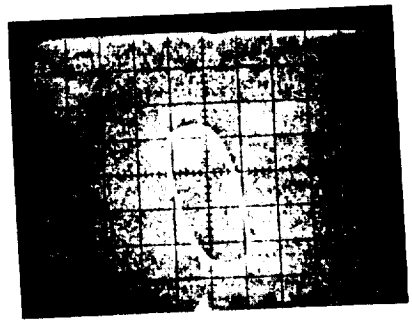

(d)

Figure 8(c). - Effect of lubricant supply pressure.

Upper four figures 5 psi
Lower four figures 45 psi